




The crystal structure of TRPM2 MHR1/2 domain reveals a conserved Zn²⁺-binding domain essential for structural integrity and channel activity

Simon Sander¹  | Jelena Pick²  | Ellen Gattkowski¹ | Ralf Fliegert² | Henning Tidow¹ 

¹Hamburg Advanced Research Centre for Bioorganic Chemistry (HARBOR) & Department of Chemistry, Institute for Biochemistry and Molecular Biology, University of Hamburg, Hamburg, Germany

²The Calcium Signaling Group, Department of Biochemistry and Molecular Cell Biology, University Medical Center Hamburg-Eppendorf, Hamburg, Germany

Correspondence

Henning Tidow, University of Hamburg, Department of Chemistry, Institute for Biochemistry and Molecular Biology, Luruper Chaussee 149, D-22761 Hamburg, Germany.
Email: tidow@chemie.uni-hamburg.de

Funding information

Deutsche Forschungsgemeinschaft, Grant/Award Numbers: A05, SFB1328

Review Editor: John Kuriyan

Abstract

Transient receptor potential melastatin 2 (TRPM2) is a Ca²⁺-permeable, non-selective cation channel involved in diverse physiological processes such as immune response, apoptosis, and body temperature sensing. TRPM2 is activated by ADP-ribose (ADPR) and 2'-deoxy-ADPR in a Ca²⁺-dependent manner. While two distinct binding sites exist for ADPR that exert different functions dependent on the species, the involvement of either binding site regarding the superagonistic effect of 2'-deoxy-ADPR is not clear yet. Here, we report the crystal structure of the MHR1/2 domain of TRPM2 from zebrafish (*Danio rerio*), and show that both ligands bind to this domain and activate the channel. We identified a so far unrecognized Zn²⁺-binding domain that was not resolved in previous cryo-EM structures and that is conserved in most TRPM channels. In combination with patch clamp experiments we comprehensively characterize the effect of the Zn²⁺-binding domain on TRPM2 activation. Our results provide insight into a conserved motif essential for structural integrity and channel activity.

KEYWORDS

2'-deoxy-ADPR, ADPR, crystal structure, electrophysiology, TRPM2, zinc

Abbreviations: 2dADPR, 2'-deoxy-adenosine diphosphate ribose; ADPR, adenosine diphosphate ribose; DMEM, Dulbecco's Modified Eagle Medium; dr, *Danio rerio* (zebrafish); EDTA, ethylenediaminetetraacetic acid; EM, electron microscopy; hs, *Homo sapiens* (human); IMAC, immobilized metal affinity chromatography; IPTG, isopropyl β-D-1-thiogalactopyranoside; ITC, isothermal titration calorimetry; MHR, TRPM homology region; NAD, nicotinamide adenine dinucleotide; Ni-NTA, Ni-nitrilotriacetic acid; NMDG, N-methyl-D-glucamine; PARG, poly-ADPR glycohydrolase; PARP, poly-ADPR polymerase; ROS, reactive oxygen species; SAD, single-wavelength anomalous diffraction; SDS-PAGE, sodium dodecyl sulfate-polyacrylamide gel electrophoresis; SD, standard deviation; TEV, tobacco etch virus; TRPM, transient receptor potential melastatin.

This is an open access article under the terms of the [Creative Commons Attribution-NonCommercial-NoDerivs](https://creativecommons.org/licenses/by-nc-nd/4.0/) License, which permits use and distribution in any medium, provided the original work is properly cited, the use is non-commercial and no modifications or adaptations are made.

© 2022 The Authors. *Protein Science* published by Wiley Periodicals LLC on behalf of The Protein Society.

1 | INTRODUCTION

Members of the melastatin subfamily of transient receptor potential channels (TRPM channels) are widely expressed and contribute to cellular Ca^{2+} signaling either directly or indirectly. They play an important role in physiological processes such as temperature sensing and regulation (TRPM8,¹ TRPM2^{2,3}), the immune response,⁴ Mg^{2+} homeostasis (TRPM6/TRPM7⁵), taste transduction (TRPM5⁶), the response to oxidative stress (TRPM2⁷) and apoptosis (TRPM2⁸). Many diseases are linked to TRPM proteins⁹ explaining the increased attention they receive as potential drug targets.^{10–12} The activity of TRPM channels is regulated by various influences such as voltage and temperature as well as changes in concentrations of small molecules, ions, or lipids (reviewed in the literature¹³). Structurally, all TRPM family members share a common core architecture: N-terminal TRPM homology regions (MHR1–4), six transmembrane helices, a TRP helix and a C-terminal coiled-coil domain.¹³

The Ca^{2+} -permeable, nonselective cation channel TRPM2, which is involved in cell death,¹⁴ diverse immune cell functions,¹⁵ temperature sensing² and the control of body temperature³ harbors a unique C-terminal domain. The name of this domain (NUDT9-H) arises from the homology to the Nudix box enzyme NUDT9, a soluble pyrophosphatase, that hydrolyzes adenosine 5'-diphosphoribose (ADPR). Due to this homology, the NUDT9-H domain was predicted to contain a binding pocket for ADPR, the endogenous ligand of TRPM2.¹⁶ Although human TRPM2 does not possess ADPR hydrolase activity,¹⁷ the recently determined structure of human TRPM2 illustrated that the NUDT9-H domain in fact binds ADPR.¹⁸ However, the cryo-EM structure of TRPM2 from zebra fish revealed a distinct ADPR-binding site in the N-terminal MHR1/2 domain.¹⁹ Since this site is conserved across TRPM2 from different species including humans, human TRPM2 harbors two distinct ADPR-binding pockets.^{18–20} The current view of gating of TRPM2 by ADPR is, that upon ADPR binding in the N-terminal domain, the clamshell-like shape of the MHR1/2 domain closes, inducing a rotation. This rotation and binding of Ca^{2+} at the membrane-cytosol interface as well as binding of a second ADPR molecule within the NUDT9-H domain lead to further conformational changes in the tetrameric channel provoking an activated state.^{18,19,21}

The cellular nucleotide ADPR is a metabolite of nicotinamide adenine dinucleotide (NAD) and can arise from the hydrolysis of NAD by the multifunctional enzyme CD38.^{22,23} Another source is poly-ADPR,

synthesized by sequential attachment of ADPR derived from NAD to proteins by the poly-ADPR polymerase (PARP). The hydrolysis of poly-ADPR and the formation of free monomeric ADPR are catalyzed by the poly-ADPR glycohydrolase (PARG) and the terminal ADPR protein glycohydrolase (TARG).²⁴ The PARP/PARG pathway is triggered by oxidative stress explaining the connection between the oxidative stress response and TRPM2.²⁵ Another TRPM2 activator is 2'-deoxy-ADPR, which proved to be a more effective TRPM2 agonist than ADPR. 2'-Deoxy-ADPR could also be detected endogenously and thus may act as second messenger.²⁶

Like a number of other Ca^{2+} channels, the human TRPM channels TRPM3, TRPM6, and TRPM7 as well as the homologous single TRPM channels from *Drosophila melanogaster* have been shown to be permeable to Zn^{2+} and to mediate Zn^{2+} entry upon activation.²⁷ While TRPM2 is inhibited by high concentration of extracellular Zn^{2+} ,²⁸ it has been shown that the cytosolic Zn^{2+} concentration in TRPM2-expressing cells increases upon activation of a photoactivatable ADPR analogue.²⁹ This indicates that TRPM channels contribute to the cellular Zn^{2+} homeostasis. Zn^{2+} is an essential trace metal that is required as a cofactor for some enzymes and as a structural component for a large number of proteins (reviewed in the literature³⁰). It has also been considered to exert signaling function and act as second messenger.³¹ Similar to Ca^{2+} , high concentrations of Zn^{2+} are cytotoxic and contribute to excitotoxicity³² and other pathological processes. A recent study of the role of TRPM2 in cell death of microglial cells showed that extracellular Zn^{2+} could also activate TRPM2 through multiple steps, involving reactive oxygen species (ROS) that induce PARP/PARG.³³ While the mechanisms remain unknown, there is evidence that also a change in the intracellular Zn^{2+} concentration influences the oxidative stress response and TRPM2.^{34,35}

Another member of the TRP family, TRPC5, comprises an intracellular Zn^{2+} -binding motif that is conserved within TRPC channels and suggests a direct modulatory role for Zn^{2+} ions on these related proteins.^{36,37}

In order to improve our understanding of the regulatory role of ADPR and 2'-deoxy-ADPR on the TRPM2 channel, we biophysically characterized ligand binding to the N-terminal MHR1/2 domain of zebrafish TRPM2 and electrophysiologically investigated possible functional consequences. The crystal structure of this domain revealed a novel Zn^{2+} -binding motif that is conserved within the TRPM family and is essential for structural integrity and activity of the channel.

2 | RESULTS AND DISCUSSION

2.1 | Biophysical and electrophysiological characterization of ADPR and 2'-deoxy-ADPR binding to drMHR1/2

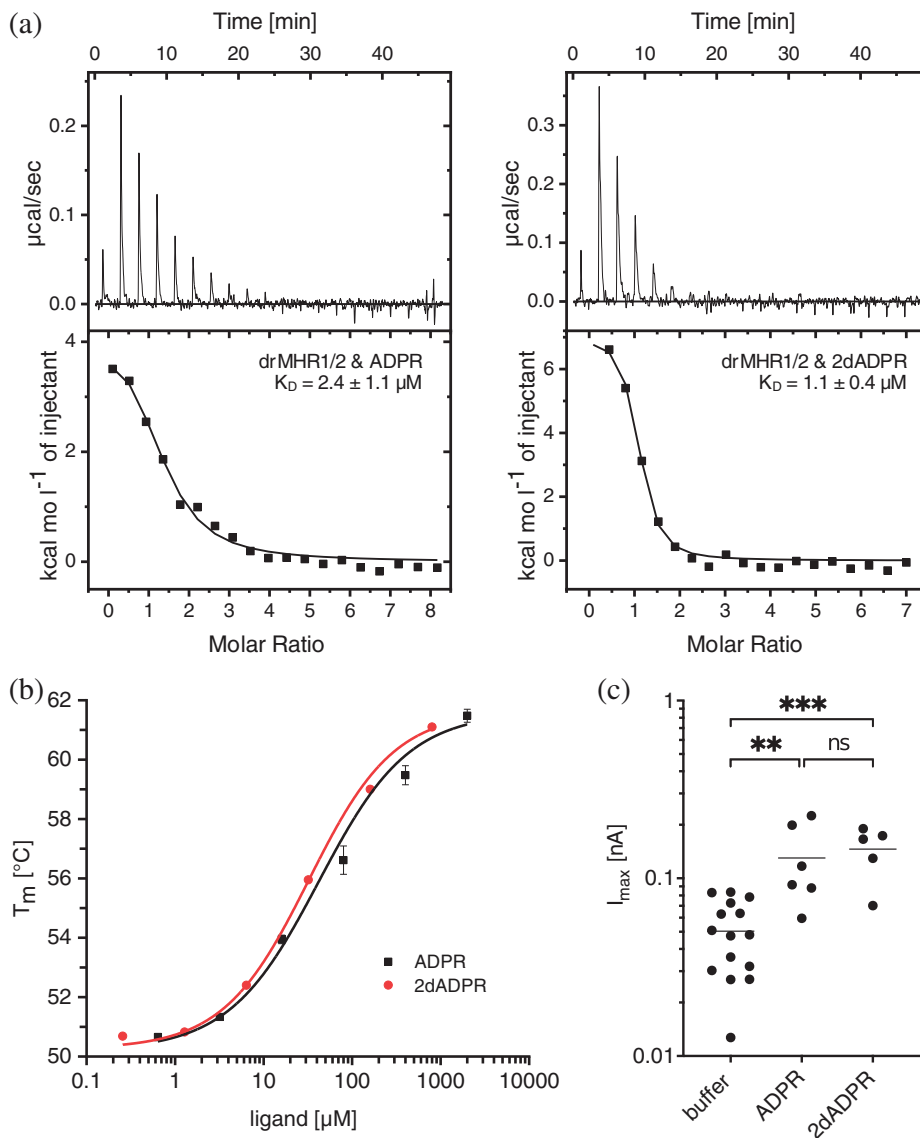
The N-terminal MHR1/2 domain of TRPM2 contains a binding site for the channel-activating ligand ADPR, which has been identified in TRPM2 cryo-EM structures from human and zebrafish.^{18,19} Whether the TRPM2 superagonist 2'-deoxy-ADPR²⁶ binds to the same site is currently unknown. In order to investigate the thermodynamic parameters of ligand binding to MHR1/2 and to confirm the structural as well as functional integrity of our sample, we determined and compared binding of ADPR and 2'-deoxy-ADPR to the isolated zebrafish

(*Danio rerio*) MHR1/2 domain (drMHR1/2) using several biophysical techniques.

Isothermal titration calorimetry (ITC) revealed endothermic binding in the low micromolar range for both ligands with 2'-deoxy-ADPR showing a slightly tighter binding than ADPR (Figure 1a). To investigate whether ligand binding has an effect on the stability of the protein, we used nano differential scanning fluorimetry (nDSF) titrations. We found that ADPR as well as 2'-deoxy-ADPR both concentration-dependently stabilize the drMHR1/2 domain (Figure 1b; Figure S1).

2'-deoxy-ADPR acts as a superagonist of human TRPM2 that induces significantly higher currents than ADPR.²⁶ The mechanisms behind the longer open times and slower inactivation caused by 2'-deoxy-ADPR are currently unknown, neither is known whether this behavior is unique to the human channel or holds true

FIGURE 1 Biophysical and electrophysiological characterization of ADPR and 2'-deoxy-ADPR binding to drMHR1/2. (a) Binding of zebrafish MHR1/2 (drMHR1/2) and ADPR/2'-deoxy-ADPR (2dADPR) as measured by isothermal titration calorimetry (ITC). K_D values are averages of triplicate experiments. (b) Binding of drMHR1/2 and ADPR/2dADPR shown by shift of melting temperature observed by differential scanning fluorimetry (nDSF). (c) Whole-cell patch clamp experiments with HEK293 cells transiently transfected with zebrafish TRPM2 (drTRPM2). Intracellular solution contained 100 nM free Ca^{2+} with 100 μ M ADPR/2dADPR or without ADPR/2dADPR (buffer control). Extracellular solution contained 100 μ M Ca^{2+} . Mean maximum currents do not differ significantly between ADPR (130 pA) and 2dADPR (146 pA).



for other orthologues as well. To address whether 2'-deoxy-ADPR also acts as a superagonist of zebrafish TRPM2 (drTRPM2), we transiently transfected HEK293 cells with an expression vector for drTRPM2 and performed whole-cell patch clamp experiments (Figure 1c, Figure S2). Under the conditions we normally use for the human channel, we observed much higher currents than with HEK293 cells transfected with human TRPM2 when ADPR was infused, in agreement with a recent report by Kühn and coworkers.³⁸ Under these conditions, most cells ruptured during the recording. We thus decided to reduce the extracellular Ca^{2+} concentration to 100 μM to reduce the driving force for Ca^{2+} and thus the positive feedback by Ca^{2+} . Under these conditions, we could follow channel activation by both ADPR and 2'-deoxy-ADPR. The maximum current during the recording does not differ significantly upon activation with ADPR or 2'-deoxy-ADPR, respectively, indicating that 2'-deoxy-ADPR does not act as a superagonist of drTRPM2. This lack of superagonist effect of 2'-deoxy-ADPR on drTRPM2 could reflect differences in the relative affinity of the MHR1/2 domain from hsTRPM2 and drTRPM2 for ADPR and 2'-deoxy-ADPR. Unfortunately, we were not able to express and purify the isolated human MHR1/2 domain in *E. coli*.

Alternatively, it could indicate a role of the second nucleotide binding site (NUDT9-H domain) in the superagonistic effect of 2'-deoxy-ADPR. In this regard, it is of interest that it has recently been shown that nvTRPM2 and drTRPM2 on one hand and hsTRPM2 on the other hand differ in their response to some ADPR analogues: Inosine 5'-diphosphoribose (IDPR), a partial agonist of human TRPM2 that is assumed to bind to the NUDT9-H domain (it is a substrate of NUDT9), does not activate drTRPM2, whereas 8-(thiophen-3-yl)-ADPR and 8-(3-acetyl-phenyl)-ADPR, analogues that act as ADPR antagonists on human TRPM2,³⁹ act as agonists of drTRPM2, implying a fundamentally different role of the two nucleotide binding sites in the human and zebrafish channel.³⁸

2.2 | Crystal structure of TRPM2 MHR1/2 domain

The TRPM2 MHR1/2 domain plays a crucial role in the regulation of the full-length channel.^{18,19,40} We determined the crystal structure of the zebrafish TRPM2 MHR1/2 domain (drMHR1/2). Two molecules were present in the asymmetric unit, with crystal contacts generated through the exposed loops. The structure was determined using Se-SAD phasing to 2.0 Å resolution

(Table S1). We could resolve almost an entire MHR1/2 domain with unambiguous side chain information (residues 33–418, with nine residues missing in the loop comprising residues 201–209). The overall structure (Figure 2a) shows a bi-lobed clamshell-like shape and superimposes well with the previously published cryo-EM structure of the full-length zebrafish TRPM2 channel (PDB: 6DRK)¹⁹ (Figure 2b,c).

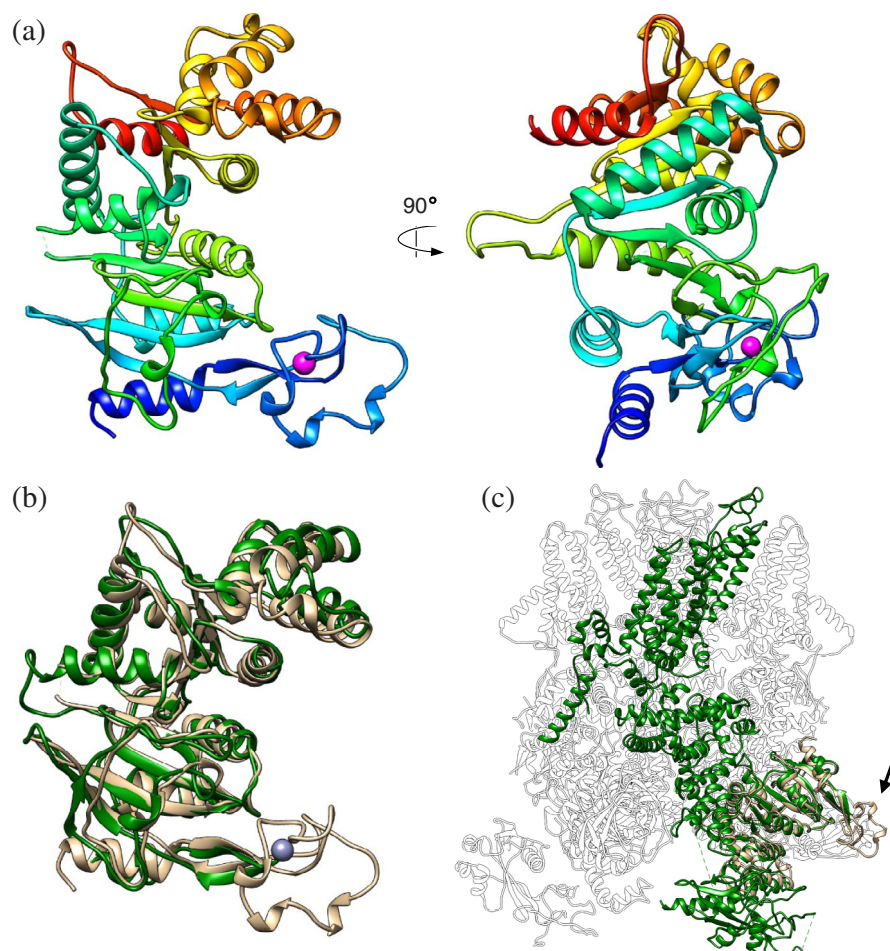
While we failed to crystallize drMHR1/2 in complex with ADPR or 2'-deoxy-ADPR, comparison with the horseshoe-like binding mode of ADPR as observed in the cryo-EM structure of ADPR-bound drTRPM2 (PDB: 6DRJ) indicates that the 2' hydroxyl group, which distinguishes ADPR and 2'-deoxy-ADPR, is solvent-exposed in the complex and thus does not contribute to the binding.¹⁹ This is in agreement with the similar binding parameters obtained for these two ligands by ITC and nDSF.

2.3 | Identification and characterization of a conserved Zn^{2+} -binding domain

The high resolution of the drMHR1/2 structure allowed unambiguous model building and identified a domain (residues 53–95), located between $\beta 1$ and $\beta 2$, which was not resolved in the lower resolution cryo-EM structure of drTRPM2.¹⁹ Surprisingly, this novel domain revealed clear electron density for an ion that is coordinated by three cysteines and one histidine (Figure 3a). The interacting residues C53, C65, C67, and H74 coordinate the ion tetrahedrally (Figure 3b) with geometry and bond length typical for Zn^{2+} ion coordination (according to *CheckMyMetal* server,⁴¹). An x-ray fluorescence energy scan of the crystal near the zinc absorption K edge (9.6586 keV) unambiguously confirmed the presence of a Zn^{2+} ion (Figure 3c).

A multiple sequence alignment revealed that the four residues forming the Zn^{2+} -binding domain (C53, C65, C67, H74) are conserved between TRPM2 orthologues from different species and most human TRPM members (Figure 3d). This strict evolutionary conservation from invertebrates to mammals strongly indicates that the novel Zn^{2+} -binding domain is physiologically relevant. As the Zn^{2+} -domain with its adjacent β -stem makes extensive interactions with the remaining MHR1/2 domain (cyan/grey interface in Figure 5), it is likely that the presence of the Zn^{2+} -binding motif causes a stabilization of the MHR1/2 domain (Figure 5). Indeed, we could show its importance for protein integrity/stability by mutating two of the cysteine residues to alanine (C65A and C67A). The mutant drMHR1/2 sequence was recombinantly expressed in *E. coli*, but

FIGURE 2 Crystal structure of drMHR1/2. (a) The overall fold of zebrafish MHR1/2 (drMHR1/2) shows a bi-lobed clamshell-like structure. The structure is colour-coded from blue (N-terminus) to red (C-terminus). Zn^{2+} ion is shown as magenta sphere. (b) Overlay of the drMHR1/2 crystal structure (wheat) with the MHR1/2 domain from a zebrafish TRPM2 (drTRPM2) cryo-EM structure (green) (PDB: 6DRK). (c) Superposition of the drMHR1/2 crystal structure (wheat) on the tetrameric drTRPM2 cryo-EM structure (white with one monomer in green), indication of the location of the novel Zn^{2+} -binding domain (PDB: 6DRK).



the protein seemed to be insoluble and thus probably incorrectly folded (Figure S3).

2.4 | The Zn^{2+} -binding domain is required for TRPM2 function

We next set out to investigate the role of the Zn^{2+} -binding domain in the context of full-length TRPM2. Full-length human TRPM2 (hsTRPM2) containing equivalent mutations of the Zn^{2+} -coordinating residues (in human: C89A and C91A) could be successfully expressed in transfected HEK293 cells and localized to the cell surface, albeit with reduced expression levels compared to the wild-type protein (Figure 4a). Whole-cell patch clamp measurements revealed that the Zn^{2+} -binding site is required for channel activity as the hsTRPM2 mutants on the cell surface with mutations of Zn^{2+} -coordinating residues did not evoke a current upon infusion of ADPR like the wild-type protein (Figure 4b, Figure S4).

Taken together, we could show that the novel motif is crucial for correct protein folding, which subsequently affects TRPM2 channel activity. Since the channel with mutations within the motif could not be activated by ADPR, an endogenous ligand of TRPM2, we postulate that the presence of an intact Zn^{2+} -domain leads to correct positioning of loop 263–273 (287–297 in hsTRPM2). This loop contains the conserved tyrosine residue Y271 (Y295 in hsTRPM2), which stacks with the adenine moiety of ADPR (see PDB: 6DRJ,¹⁹). In this model, the stabilization and loop positioning caused by the Zn^{2+} -domain primes the MHR1/2 domain for ligand binding (Figure 5).

Interestingly, a structurally similar Cys_3 - His_1 Zn^{2+} -binding motif has recently been discovered in the N-terminal region of human TRPC5.³⁷ While being nonrelated in sequence to our motif identified in TRPM channels, this motif is also conserved across all TRPC channels, indicating that both TRPM and TRPC channels contain a conserved intracellular Zn^{2+} -binding site.

3 | MATERIALS AND METHODS

3.1 | Key resources table

Reagent type (species) or resource	Designation	Source or reference	Identifiers
Gene	TRPM2	GenScript	ODa47363D
Strain, strain background (<i>E. coli</i>)	BL21 Gold (DE3)	Agilent	230132
Strain, strain background (<i>E. coli</i>)	B834 (DE3)	Merck	69041
Cell line, human	HEK293	ATCC	CRL-1573
Chemical compound	L selenomethionine	Serva	77765.01
Chemical compound	ADPR	Sigma-Aldrich	A0752
Chemical compound	2'-deoxy-ADPR	BioLog	D 227-01
Software, algorithm	XDS	42	http://xds.mpimf-heidelberg.mpg.de/
Software, algorithm	AIMLESS	43	http://www.ccp4.ac.uk/html/aimless.html
Software, algorithm	SHELXCD	44	https://shelx.uni-goettingen.de/
Software, algorithm	ARP/wARP	45	https://www.embl-hamburg.de/ARP/
Software, algorithm	Coot 0.8.9.1	46	https://www2.mrc-lmb.cam.ac.uk/personal/pemsley/coot/
Software, algorithm	PHENIX 1.16	47	https://www.phenix-online.org/
Software, algorithm	Clustal Omega	48	https://www.ebi.ac.uk/Tools/msa/clustalo/

3.2 | Materials

All chemicals were of analytical grade and obtained from Roth (Karlsruhe, Germany) or Sigma Aldrich/Merck (Darmstadt, Germany).

3.3 | Protein expression and purification

The sequence coding for the zebrafish TRPM2 MHR1/2 domain (drMHR1/2, residues 1–419 of drTRPM2) was cloned into a pNEK-vH vector bearing a TEV-cleavable N-terminal His₆-tag. Protein production was carried out in *E. coli* BL21 Gold (DE3) cells in Terrific Broth (TB) media supplemented with 25 µg/ml kanamycin. Cells were grown at 37°C until a cell density of 1 (measured at 600 nm) was reached. After induction with 0.1 mM isopropyl β-D-1-thiogalactopyranoside (IPTG), the cells were grown for further 16 hr at 20°C. The production of selenomethionine-labeled protein was carried out in the methionine auxotroph *E. coli* strain B834⁴² in M9 minimal medium supplemented with 70 mg/L L-selenomethionine (Serva) and 25 µg/ml kanamycin. Cells were grown at 37°C to an OD₆₀₀ of 0.6 and after induction with 0.1 mM IPTG, the target protein was expressed for further 16 hr at 20°C.

The cells were harvested by centrifugation (5,000g for 25 min) and lysed in 25 mM Tris pH 7.5, 300 mM NaCl, 5% (v/v) glycerol, 5 mM 2-mercaptoethanol using a high-pressure homogenizer (EmulsiFlex-C3, Avestin). Cell

debris was removed by centrifugation (39,000g for 45 min) and the His₆-tagged protein was purified from the supernatant using immobilized metal affinity chromatography (IMAC) with Ni-NTA resin (Roth). After His-tag removal by TEV protease (1/10 w:w) and reverse Ni-NTA purification, the target protein was further purified by gel filtration on a Superdex S200 increase 10/300 column using buffer M (for wild-type protein, 25 mM HEPES pH 7.5, 150 mM NaCl, 5 mM CaCl₂, 5 mM MgCl₂) or buffer MS (for Se-Met-labeled protein, 25 mM HEPES pH 7.5, 150 mM NaCl, 5 mM CaCl₂, 5 mM MgCl₂, 5 mM 2-mercaptoethanol). Peak fractions were pooled and protein identity confirmed by SDS-PAGE and mass spectrometry.

3.4 | Isothermal titration calorimetry

ITC measurements were carried out at 25°C using a MicroCal ITC-200 isothermal titration calorimeter (Malvern Panalytical) and thermodynamic parameters were analyzed using the MicroCal ORIGIN™ software. The ligands ADPR and 2'-deoxy ADPR were each dissolved in buffer M (see purification) to a concentration of 500 µM and placed in the syringe. After an initial injection of 0.5 µl, 18 regular injections of 2 µl were added to

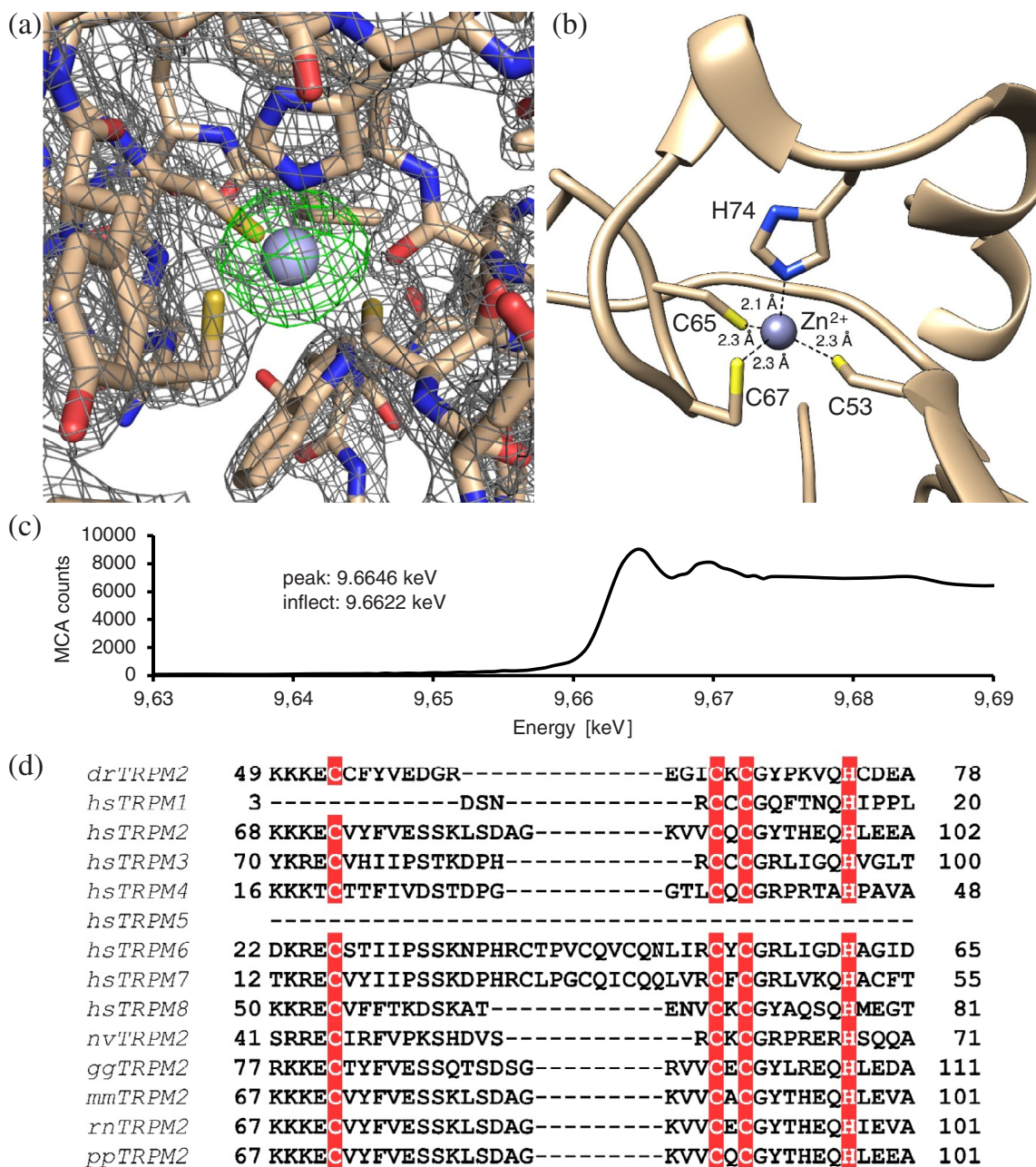


FIGURE 3 Novel Zn²⁺-binding domain in drMHR1/2 that is conserved in TRPM channels. (a) Electron density of the novel Zn²⁺-binding site (grey mesh) and PHENIX POLDER electron density after omission of the Zn²⁺ ion (green mesh) with the atomic model (wheat) and the Zn²⁺ ion (grey). (b) Detailed structure view of the Zn²⁺-binding domain with a tetrahedral coordination of the Zn²⁺ ion by C53, C65, C67, H74. (c) X-ray energy scan of the fluorescence emitted by the sample near the zinc absorption K edge (9.6586 keV) confirming ion identity. (d) Multiple sequence alignment of novel Zn²⁺-binding domain in TRPM channels. Conservation of the four Zn²⁺-coordinating residues (marked) in the N-terminus of most TRPM channels. Alignment of all human (*Homo sapiens*) TRPM channels and TRPM2 from sea starlet anemone (*Nematostella vectensis*), chicken (*Gallus gallus*), mouse (*Mus musculus*), rat (*Rattus norvegicus*), chimpanzee (*Pan pansicus*), zebrafish (*Danio rerio*).

10 μ M drMHR1/2 in the sample cell. The individual injections were interspaced by 150 s and stirring speed was set to 750 rpm. Heat of dilution was obtained by titrating ADPR into buffer M and baseline corrections were carried out accordingly. All ITC experiments were performed as triplicates and errors are reported as standard deviations of the mean K_D value.

3.5 | Differential scanning fluorimetry

nDSF measurements were carried out on a Prometheus NT.48 system (Nanotemper). The 10 μ M drMHR1/2 protein was mixed with varying amounts (600 nM to 2 mM) of ADPR or 2'-deoxy ADPR in buffer M (see purification). Thermal unfolding was measured by following intrinsic

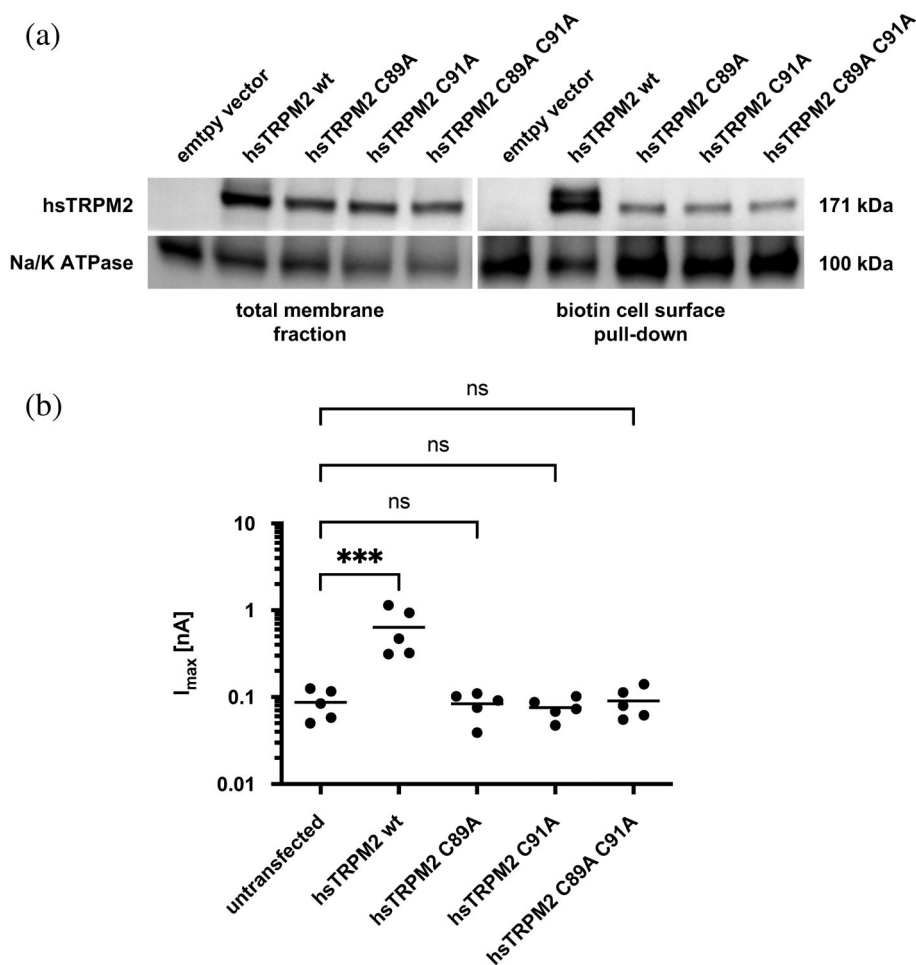


FIGURE 4 The novel Zn^{2+} -binding site in the MHR1/2 domain is important for protein integrity and TRPM2 channel activity. (a) Cell surface biotinylation assay with Zn^{2+} -binding site mutants of human TRPM2 (hsTRPM2) proving the importance of the motif. The expression level of the mutants is lower on the cell surface and in the total membrane fraction. (b) Whole-cell patch clamp measurements showing that the Zn^{2+} -binding site is also important for channel activity. The remaining fraction of mutant protein on the cell surface of HEK293 cells transfected with hsTRPM2 variants does not invoke a current upon infusion of 200 nM free Ca^{2+} with 100 μM ADPR via the patch pipette. The extracellular solution contained 1 mM Ca^{2+} .

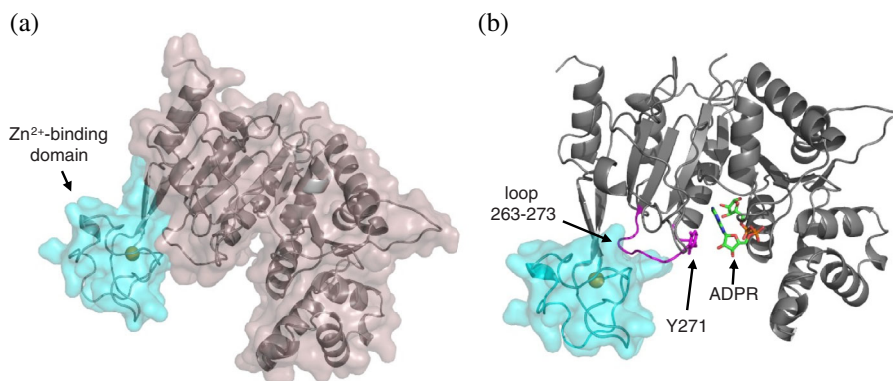


FIGURE 5 Importance of Zn-binding domain for MHR1/2 stability and ADPR binding. (a) Zn^{2+} -binding domain (cyan) makes substantial interactions with the remaining part of the MHR1/2 domain (grey). (b) The presence of the Zn^{2+} -binding domain in drMHR1/2 leads to correct positioning of loop 263–273 (magenta) containing the conserved tyrosine residue Y271 which stacks with the adenine moiety of ADPR (see PDB:6DRJ,¹⁹). According to this model, the stabilization and loop positioning caused by the Zn^{2+} -domain primes the MHR1/2 domain for ligand binding.

tryptophan fluorescence during a thermal ramp (1°C/min). The PR.ThermControl software (Nanotemper) was used to determine melting temperatures. Binding parameter analysis was performed by simple Hill fit in the ORIGIN™ software.

3.6 | Crystallization

Crystals of selenomethionine-labeled drMHR1/2 protein were grown by sitting drop vapor diffusion technique. The 1 μl of purified protein (4 mg/ml) was mixed with

1 μ l of the precipitant mix (Tris, BICINE, diethylene glycol, triethylene glycol, tetraethylene glycol, pentaethylene glycol, glycerol; PEG4000, Jeffamine M-600). Crystals of triangular shape appeared after 1–3 days, reaching sizes of approximately 50–120 μ m.

3.7 | Structure determination

X-ray diffraction data were collected at 100 K at the PETRA III/EMBL P14 beamline. All datasets were processed with XDS⁴³ and merged with AIMLESS.⁴⁴ Heavy atom site identification and phasing was performed with SHELXC.D.⁴⁵ A combination of ARP/wARP⁴⁶ and COOT⁴⁷ was used for automatic and manual model building, respectively. Refinement was carried out in PHENIX.⁴⁸ The final model corresponds to residues 38–423. All data collection and refinement statistics are summarized in Table S1 (supplementary information).

3.8 | Multiple sequence alignment

Multiple sequence alignment of TRPM2 and homologues was performed using the Clustal Omega server.⁴⁹ Results were visualized with Jalview (<https://www.jalview.org/>).

3.9 | Cell culture and transfection vectors

HEK293 wild type cells were cultivated in Dulbecco's modified eagle medium (DMEM) (with GlutaMAX-I, 4.5 g/L D-Glucose and Phenol Red; Gibco) supplemented with 10% FBS (Sigma), 100 U/ml Penicillin and 100 μ g/ml Streptomycin (Gibco) and kept at 37°C and 5% CO₂.

Cells were transiently transfected with pIRES2-EGFP expression vectors containing either full-length human TRPM2 variants (wild type, C89A, C91A, C89A C91A double mutant) or full-length zebrafish TRPM2 (wild type). Transfection was verified by fluorescence microscopy.

3.10 | Cell surface biotinylation assay

Transfection of hsTRPM2 variants or empty vector was performed with Lipofectamine LTX (Thermo Fisher) according to the manufacturer's instructions. Cells were grown for 48 hr after transfection, washed with D-PBS (Gibco) and incubated with 1 mg/ml EZ-Link Sulfo-NHS-LC-Biotin (Thermo Fisher) in order to biotinylate cell surface proteins. After detachment with 2 mM EDTA in

D-PBS, the cells were collected, centrifuged (500 g for 5 min) and washed with D-PBS. Cell lysis and membrane protein extraction was performed using the ProteoExtract Native Membrane kit (Merck Millipore) according to the manufacturer's protocol. Solubilized membrane protein samples were quantified by Bradford assay.

NeutraVidin Agarose beads (70 μ l, Thermo Fisher) were used to isolate the biotinylated cell surface proteins. The beads were incubated with total membrane protein samples (600 μ g) for 18 hr while rotating at 4°C. After washing with extraction buffer II from the kit mentioned above, the beads and the total membrane protein samples were mixed with SDS sample buffer (with 5% 2-mercapto ethanol) and heated to 75°C for 5 min.

The samples were analyzed by western blot. After SDS-PAGE (4%–20% Protean precast gel, BioRad) and transfer to a polyvinylidene difluoride membrane (Merck Millipore), the membrane was cut at 140 kDa in order to simultaneously detect TRPM2 (171 kDa) and the reference Na⁺/K⁺-ATPase (100 kDa). The membrane parts were probed for 18 hr with anti-hsTRPM2 antibody from rabbit (Novus #nb500-241 at 1:50,000 dilution) and anti-Na⁺/K⁺-ATPase antibody from rabbit (Cell Signaling #3010 at 1:1000 dilution), respectively. Both primary antibodies were detected with an HRP-conjugated anti-rabbit secondary antibody (Dianova #111-035-045 at 1:10,000 dilution) for 1 h. Chemiluminescent detection was performed using the SuperSignal West Pico substrate (Thermo Fisher).

3.11 | Electrophysiology (patch clamp)

3.11.1 | hsTRPM2

HEK293 cells were transfected 24 hr prior to experiments using jetPEI reagent (Polyplus transfection). The transfection complex (5 μ g DNA and 10 μ l jetPEI reagent in 150 mM NaCl solution at a total volume of 250 μ l) was incubated for 30 min before 2.5×10^5 cells were added. The cell suspension was subsequently seeded to 35 mm dishes at low density. Patch clamp experiments were performed at room temperature. Before the start of the experiments the medium was replaced by extracellular solution (in mM: 140 *N*-methyl-D-glucamine [NMDG], 5 KCl, 3.3 MgCl₂, 1 CaCl₂, 5 D-Glucose, 10 HEPES, adjusted to pH 7.4 with HCl). Patch pipettes were pulled from 1.05 \times 1.50 \times 80 mm glass capillaries and filled with intracellular solution (in mM: 0.1 ADPR, 120 KCl, 8 NaCl, 1 MgCl₂, 10 HEPES, adjusted to pH 7.2 with KOH; The intracellular Ca²⁺ concentration was set to 200 nM with 10 mM EGTA and 5.6 mM CaCl₂, as calculated with Maxchelator.). After pipette resistances were

determined (1.5–2.9 M Ω), currents were compensated for fast and slow capacity transients and recorded in whole-cell configuration. The series resistance compensation was set to 70%. Using voltage clamp, repetitive voltage ramps of 140 ms spanning the range from –85 mV to +20 mV were applied from a holding potential of –50 mV every 5 s over a measuring period of 445 s. For data analysis, the maximum outward current at +15 mV of each measuring period was extracted from all experiments. Cells with a series resistance >10 M Ω during the experiment were excluded from data analysis.

3.11.2 | drTRPM2

Cells were transfected with jetPEI reagent as described above (transfection complex: 1 μ g DNA and 5 μ l jetPEI reagent in 150 mM NaCl solution at a total volume of 250 μ l). Due to large whole-cell currents and subsequent rupturing of the cells, the patch clamp protocol was adjusted for drTRPM2. Compared to human TRPM2, zebrafish TRPM2 has a higher permeability for Ca²⁺.⁵⁰ To reduce Ca²⁺ inward current and thus positive feedback by Ca²⁺, the Ca²⁺ concentration in the extracellular solution was reduced to 100 μ M. Additionally, the Ca²⁺ concentration in the intracellular solution was reduced to 100 nM. The holding potential was set to –40 mV. Since under these Ca²⁺-reduced conditions, whole-cell currents were still too high, only cells with relatively low drTRPM2 expression levels were measured. The drTRPM2 expression level was quantified by measuring the EGFP fluorescence intensity. Using a fluorescence filter, a picture of each cell was taken prior to the experiment (Leica DMI8 microscope). The exposure time was set to 1,000 ms. EGFP Fluorescence intensities are given as gray-level values and are the same in each measuring group (image analysis with ImageJ) (Figure S2C).

3.12 | Statistical analysis

Statistical analysis was performed with GraphPad Prism (v9, GraphPad Software). After normal distribution was confirmed by Kolmogorov–Smirnov test, one-way ANOVA test was applied followed by Dunnett (for hsTRPM2) and Tukey (for drTRPM2) test for multiple comparisons.

ACKNOWLEDGMENTS

The authors are grateful to the staff at beamlines P14 and P13 (EMBL, Hamburg) and thank members of the Tidow and Fliegert labs for helpful discussions. The authors acknowledge access to the Sample Preparation

and Characterization (SPC) Facility of EMBL, Hamburg. This work was supported by the Deutsche Forschungsgemeinschaft (DFG) (SFB1328, project A05 to Henning Tidow and Ralf Fliegert). Open Access funding enabled and organized by Projekt DEAL.

AUTHOR CONTRIBUTIONS

Simon Sander: Conceptualization (equal); data curation (lead); investigation (lead); methodology (equal); visualization (equal); writing – original draft (equal); writing – review and editing (equal). **Jelena Pick:** Data curation (supporting); investigation (equal); methodology (supporting); visualization (supporting); writing – original draft (supporting); writing – review and editing (supporting). **Ellen Gattkowski:** Investigation (supporting). **Ralf Fliegert:** Conceptualization (equal); funding acquisition (equal); investigation (equal); project administration (equal); supervision (equal); writing – original draft (equal); writing – review and editing (equal). **Henning Tidow:** Conceptualization (equal); funding acquisition (equal); investigation (equal); project administration (lead); resources (equal); supervision (lead); writing – original draft (equal); writing – review and editing (equal).

CONFLICT OF INTEREST

The authors declare no competing financial interest.

DATA AVAILABILITY STATEMENT

Structural coordinates and structural factors have been deposited in the RCSB Protein Data Bank under accession number 7AOV (see Suppl. Table 1).

ORCID

Simon Sander  <https://orcid.org/0000-0002-7985-2526>

Jelena Pick  <https://orcid.org/0000-0002-9281-1155>

Henning Tidow  <https://orcid.org/0000-0002-4702-9332>

REFERENCES

1. McKemy DD, Neuhausser WM, Julius D. Identification of a cold receptor reveals a general role for TRP channels in thermosensation. *Nature*. 2002;416:52–58.
2. Tan CH, McNaughton PA. The TRPM2 ion channel is required for sensitivity to warmth. *Nature*. 2016;536:460–463.
3. Siemens J, Pohle J, Wang H, et al. The TRPM2 channel is a hypothalamic heat sensor that limits fever and can drive hypothermia. *Science* (80-). 2016;. 353:1393–1398.
4. Schmitz C, Perraud A-L. The TRPM cation channels in the immune context. *Curr Pharm Des*. 2005;11:2765–2778.
5. Montell C. Mg²⁺ homeostasis: The Mg²⁺-nifent TRPM channels. *Curr Biol*. 2003;13:799–801.
6. Pérez CA, Huang L, Rong M, et al. A transient receptor potential channel expressed in taste receptor cells. *Nat Neurosci*. 2002;5:1169–1176.

7. Simon F, Varela D, Cabello-Verrugio C. Oxidative stress-modulated TRPM ion channels in cell dysfunction and pathological conditions in humans. *Cell Signal*. 2013;25:1614–1624.
8. McNulty S, Fonfria E. The role of TRPM channels in cell death. *Pflugers Arch Eur J Physiol*. 2005;451:235–242.
9. Jimenez I, Prado Y, Marchant F, et al. TRPM channels in human diseases. *Cells*. 2020;9:2604.
10. Abriel H, Syam N, Sottas V, Amarouch MY, Rougier J-S. TRPM4 channels in the cardiovascular system: Physiology, pathophysiology, and pharmacology. *Biochem Pharmacol*. 2012;84:873–881.
11. Sun Y, Sukumaran P, Schaar A, Singh BB. TRPM7 and its role in neurodegenerative diseases. *Channels*. 2015;9:253–261.
12. Vennekens R, Mesuere M, Philippaert K. TRPM5 in the battle against diabetes and obesity. *Acta Physiol*. 2018;222:e12949.
13. Huang Y, Fliegert R, Guse AH, Lü W, Du J. A structural overview of the ion channels of the TRPM family. *Cell Calcium*. 2020;85:102111.
14. Hecquet CM, Zhang M, Mittal M, et al. Cooperative interaction of trp melastatin channel transient receptor potential (TRPM2) with its splice variant TRPM2 short variant is essential for endothelial cell apoptosis. *Circ Res*. 2014;114:469–479.
15. Knowles H, Heizer JW, Li Y, et al. Transient receptor potential Melastatin 2 (TRPM2) ion channel is required for innate immunity against *Listeria monocytogenes*. *Proc Natl Acad Sci*. 2011;108:11578–11583.
16. Perraud AL, Fleig A, Dunn CA, et al. ADP-ribose gating of the calcium-permeable LTRPC2 channel revealed by Nudix motif homology. *Nature*. 2001;411:595–599.
17. Iordanov I, Mihályi C, Tóth B, Csanády L. The proposed channel-enzyme transient receptor potential melastatin 2 does not possess ADP ribose hydrolase activity. *Elife*. 2016;5:1–20.
18. Huang Y, Roth B, Lü W, Du J. Ligand recognition and gating mechanism through three ligand-binding sites of human TRPM2 channel. *Elife*. 2019;8:1–18.
19. Huang Y, Winkler PA, Sun W, Lü W, Du J. Architecture of the TRPM2 channel and its activation mechanism by ADP-ribose and calcium. *Nature*. 2018;562:145–149.
20. Wang L, Fu T-M, Zhou Y, Xia S, Greka A, Wu H. Structures and gating mechanism of human TRPM2. *Science*. 2018;362:eaav4809.
21. Yin Y, Wu M, Hsu AL, et al. Visualizing structural transitions of ligand-dependent gating of the TRPM2 channel. *Nat Commun*. 2019;10:3740.
22. Howard M, Grimaldi J, Bazan J, et al. Formation and hydrolysis of cyclic ADP-ribose catalyzed by lymphocyte antigen CD38. *Science (80-)*. 1993;262:1056–1059.
23. Zocchi E, Franco L, Guida L, et al. A single protein immunologically identified as CD38 displays NAD⁺ Glycohydrolase, ADP-Ribosyl cyclase and cyclic ADP-ribose hydrolase activities at the outer surface of human erythrocytes. *Biochem Biophys Res Commun*. 1993;196:1459–1465.
24. Nikiforov A, Kulikova V, Ziegler M. The human NAD metabolome: Functions, metabolism and compartmentalization. *Crit Rev Biochem Mol Biol*. 2015;50:284–297.
25. Buelow B, Song Y, Scharenberg AM. The poly(ADP-ribose) polymerase PARP-1 is required for oxidative stress-induced TRPM2 activation in lymphocytes. *J Biol Chem*. 2008;283:24571–24583.
26. Fliegert R, Bauche A, Wolf Pérez AM, et al. 2'-deoxyadenosine 5'-diphosphoribose is an endogenous TRPM2 superagonist. *Nat Chem Biol*. 2017;13:1036–1044.
27. Bouron A, Oberwinkler J. Contribution of calcium-conducting channels to the transport of zinc ions. *Pflugers Arch Eur J Physiol*. 2014;466:381–387.
28. Yang W, Manna PT, Zou J, et al. Zinc inactivates melastatin transient receptor potential 2 channels via the outer pore. *J Biol Chem*. 2011;286:23789–23798.
29. Yu P, Wang Q, Zhang LH, Lee HC, Zhang L, Yue J. A cell permeable NPE caged ADP-ribose for studying TRPM2. *PLoS One*. 2012;7:e51028.
30. Kambe T, Tsuji T, Hashimoto A, Itsumura N. The physiological, biochemical, and molecular roles of zinc transporters in zinc homeostasis and metabolism. *Physiol Rev*. 2015;95:749–784.
31. Fukada T, Yamasaki S, Nishida K, Murakami M, Hirano T. Zinc homeostasis and signaling in health and diseases. *J Biol Inorg Chem*. 2011;16:1123–1134.
32. Granzotto A, Canzoniero LMT, Sensi SL. A neurotoxic Ménage-à-trois: Glutamate, calcium, and zinc in the excitotoxic cascade. *Front Mol Neurosci*. 2020;13:1–13.
33. Mortadza SS, Sim JA, Stacey M, Jiang LH. Signalling mechanisms mediating Zn²⁺-induced TRPM2 channel activation and cell death in microglial cells. *Sci Rep*. 2017;7:1–15.
34. Abuarab N, Munsey TS, Jiang LH, Li J, Sivaprasadarao A. High glucose-induced ROS activates TRPM2 to trigger lysosomal membrane permeabilization and Zn²⁺-mediated mitochondrial fission. *Sci Signal*. 2017;10:1–12.
35. Ye M, Yang W, Ainscough JF, et al. TRPM2 channel deficiency prevents delayed cytosolic Zn²⁺ accumulation and CA1 pyramidal neuronal death after transient global ischemia. *Cell Death Dis*. 2014;5:e1541.
36. Park SE, Song JH, Hong C, et al. Contribution of zinc-dependent delayed calcium influx via TRPC5 in oxidative neuronal death and its prevention by novel TRPC antagonist. *Mol Neurobiol*. 2019;56:2836–2837.
37. Wright DJ, Simmons KJ, Johnson RM, Beech DJ, Muench SP, Bon RS. Human TRPC5 structures reveal interaction of a xanthine-based TRPC1/4/5 inhibitor with a conserved lipid binding site. *Commun Biol*. 2020;3:704.
38. Kühn FJP, Ehrlich W, Barth D, Kühn C, Lückhoff A. Functional importance of NUDT9H domain and N-terminal ADPR-binding pocket in two species variants of vertebrate TRPM2 channels. *Sci Rep*. 2019;9:19224.
39. Moreau C, Kirchberger T, Swarbrick JM, et al. Structure-activity relationship of adenosine 5'-diphosphoribose at the transient receptor potential melastatin 2 (TRPM2) channel: Rational design of antagonists. *J Med Chem*. 2013;56:10079–10102.
40. Tóth B, Iordanov I, Csanády L. Selective profiling of N- and C-terminal nucleotide-binding sites in a TRPM2 channel. *J Gen Physiol*. 2020;152:1–13.
41. Zheng H, Cooper DR, Porebski PJ, Shabalin IG, Handing KB, Minor W. CheckMyMetal: A macromolecular metal-binding validation tool. *Acta Crystallogr. Sect. D. Struct Biol*. 2017;73:223–233.
42. Wood WB. Host specificity of DNA produced by *Escherichia coli*: Bacterial mutations affecting the restriction and modification of DNA. *J Mol Biol*. 1966;16:118–133.
43. Kabsch W. XDS. *Acta Crystallogr D Biol Crystallogr*. 2010;66:125–132.

44. Evans PR, Murshudov GN. How good are my data and what is the resolution? *Acta Crystallogr Sect D Biol Crystallogr*. 2013; 69:1204–1214.
45. Sheldrick GM. A short history of SHELX. *Acta Crystallogr Sect A Found Crystallogr*. 2008;64:112–122.
46. Langer G, Cohen SX, Lamzin VS, Perrakis A. Automated macromolecular model building for X-ray crystallography using ARP/wARP version 7. *Nat Protoc*. 2008;3:1171–1179.
47. Emsley P, Lohkamp B, Scott WG, Cowtan K. Features and development of coot. *Acta Crystallogr Sect D Biol Crystallogr*. 2010;66:486–501.
48. Liebschner D, Afonine PV, Baker ML, et al. Macromolecular structure determination using X-rays, neutrons and electrons: Recent developments in Phenix. *Acta Crystallogr Sect D Struct Biol*. 2019;75:861–877.
49. Madeira F, Park YM, Lee J, et al. The EMBL-EBI search and sequence analysis tools APIs in 2019. *Nucleic Acids Res*. 2019; 47:W636–W641.
50. Fliegert R, Hölzer HT, Guse AH. TRPM2 activation: Paradigm shifted? *Cell Calcium*. 2018;76:132–134.

SUPPORTING INFORMATION

Additional supporting information may be found in the online version of the article at the publisher's website.

How to cite this article: Sander S, Pick J, Gattkowsky E, Fliegert R, Tidow H. The crystal structure of TRPM2 MHR1/2 domain reveals a conserved Zn²⁺-binding domain essential for structural integrity and channel activity. *Protein Science*. 2022;31(6):e4320. <https://doi.org/10.1002/pro.4320>